

CuMn-V compounds: a transition from semimetal low-temperature to semiconductor high-temperature antiferromagnets

F. Máca,¹ J. Mašek,¹ O. Stelmakhovych,² X. Martí,² K. Uhlířová,²
P. Beran,³ H. Reichlová,⁴ P. Wadley,⁴ V. Novák,⁴ and T. Jungwirth^{4,5}

¹*Institute of Physics ASCR, v.v.i., Na Slovance 2, 182 21 Praha 8, Czech Republic*

²*Faculty of Mathematics and Physics, Charles University in Prague,
Ke Karlovu 3, 121 16 Prague 2, Czech Republic*

³*Nuclear Physics Institute ASCR, v.v.i., 250 68 Řež, Czech Republic*

⁴*Institute of Physics ASCR, v.v.i., Cukrovarnická 10, 162 53 Praha 6, Czech Republic*

⁵*School of Physics and Astronomy, University of Nottingham, Nottingham NG7 2RD, United Kingdom*

(Dated: November 10, 2021)

We report on a theoretical and experimental study of CuMn-V antiferromagnets. Previous works showed low-temperature antiferromagnetism and semimetal electronic structure of the semi-Heusler CuMnSb. In this paper we present theoretical predictions of high-temperature antiferromagnetism in the stable orthorhombic phases of CuMnAs and CuMnP. The electronic structure of CuMnAs is at the transition from a semimetal to a semiconductor and we predict that CuMnP is a semiconductor. We show that the transition to a semiconductor-like band structure upon introducing the lighter group-V elements is present in both the metastable semi-Heusler and the stable orthorhombic crystal structures. On the other hand, the orthorhombic phase is crucial for the high Néel temperature. Results of X-ray diffraction, magnetization, transport, and neutron diffraction measurements we performed on chemically synthesized CuMnAs are consistent with the theory predictions.

PACS numbers: 71.22.+i, 81.15.Hi, 75.50.Pp

I. INTRODUCTION

Recent observation of a large magnetoresistance in an antiferromagnet (AFM) based spin-valve opens the prospect for utilizing AFMs in spintronics.^{1,2} Particularly appealing is the introduction of AFMs into semiconductor spintronics because of the lack of suitable high-temperature ferromagnetic (FM) semiconductors. In Tab I we show a survey of the magnetic counterparts of the most common II-VI and III-V compound semiconductors, and of the related I-VI-III-VI and II-V-IV-V families, in which Mn (Eu) acts as a group-II atom and Fe (Gd) as a group-III element. The table illustrates that AFM ordering occurs much more frequently than FM ordering. Yet, only a few of these AFM semiconductors have Néel temperatures T_N above the room temperature. In MnTe, $T_N = 323$ K is presumably still too low to allow for room-temperature applications of the material in spintronics. MnSiN₂ appears as an attractive candidate material which should also allow for the application of common molecular beam epitaxy techniques for the synthesis of high quality films. The natural mineral CuFeS₂ is more challenging from the perspective of the epitaxial growth because of the vastly different vapor pressures of S and the noble and transition metals. Another limiting factor is that both MnSiN₂ and CuFeS₂ might be the only high- T_N AFMs in their respective semiconductor compound families.

The search for other high temperature AFM semiconductors has recently resulted in a report of the semiconducting band structure of I(a)-Mn-V compounds and of the successful synthesis of single-crystal LiMnAs by molecular beam epitaxy.¹⁶ In contrast to the other com-

II-VI	T_c (K)	T_N (K)	III-V	T_c (K)	T_N (K)
MnO		122 ³	FeN		100 ⁴
MnS		152 ⁵	FeP		115 ⁶
MnSe		173 ³	FeAs		77 ⁷
MnTe		323 ³	FeSb		100-220 ⁸
EuO	67	³	GdN	72	³
EuS	16	³	GdP		15 ⁹
EuSe		5 ³	GdAs		19 ¹⁰
EuTe		10 ³	GdSb		27 ¹¹
I-VI-III-VI			II-V-IV-V		
CuFeO ₂		11 ¹²	MnSiN ₂		490 ¹³
CuFeS ₂		825 ³			
CuFeSe ₂		70 ¹⁴			
CuFeTe ₂		254 ¹⁵			

TABLE I: Comparison of FM Curie temperatures (T_c) and AFM Néel temperatures (T_N) of II-VI, I-VI-III-VI, III-V, and II-V-IV-V magnetic semiconductors.

mon semiconductor compound families, many of the I(a)-Mn-V semiconductors are room-temperature AFMs.^{17,18} While favorable from the perspective of their electronic band structure and magnetic characteristics, the utility of I(a)-Mn-V materials in devices may represent a challenge due to the high reactivity and diffusivity of the I(a) alkali metals elements. The aim of this paper is to investigate the noble-metal group-I(b) counterparts of these compounds. In particular, we focus on CuMnAs and CuMnP.

The anticipation of semiconducting band structure of

the high-temperature AFM LiMnAs (and other I(a)-Mn-V's) was based on the picture of Li^{1+} charge state as in Zintl compounds, Mn^{2+} charge state as observed in (Ga,Mn)As and some other (III,Mn)V and (II,Mn)VI magnetic semiconductors, and the established close relationship between non-magnetic I(a)-II-V and III-V semiconductors.¹⁶ From this viewpoint, the $\text{Cu}^{1+}\text{Mn}^{2+}\text{Sb}^{3-}$ configuration inferred from previous density functional theory studies¹⁹ of this semi-Heusler alloy hints that the replacement of the I(a) alkali-metal with the I(b) Cu in I-Mn-V compounds is a promising approach. Although not a semiconductor, CuMnSb is also not a conventional metal with a high density of states at the Fermi energy but rather a semimetal with a small overlap between the bottom of the conduction band and the top of the valence band.^{19,20} The relatively low room-temperature conductivity of $\sim 6 \times 10^3 \Omega^{-1}\text{cm}^{-1}$ measured in this compound supports the theoretically predicted semimetal band-structure.²¹ By introducing a lighter group-V element As or P, one may expect the band-gap to fully open.

In the literature, CuMnSb is often quoted as a rare example among semi-Heusler alloys with AFM order.¹⁹⁻²⁵ It has a Néel temperature of 50 K. Synthesis and crystal structure measurements of CuMnAs and CuMnP were reported in Ref. 26. Unlike the cubic CuMnSb, the equilibrium crystal structure of CuMnAs and CuMnP is orthorhombic Pnma. Susceptibility measurements of CuMnAs presented in Ref. 26 indicate possible AFM order at room temperature. To the best of our knowledge, the electronic and magnetic structure of CuMnAs and CuMnP has not been further investigated experimentally and no band structure calculations have been published to date. In this paper we present full-potential density functional theory calculations of the electronic and magnetic structure of CuMnAs and CuMnP. We complement the theory analysis by X-ray diffraction, magnetization, transport, and neutron diffraction measurements of chemically synthesized CuMnAs. As a reference, we also report our experimental results on CuMnSb.

II. THEORY

To calculate the electronic structure of CuMn-V compounds we employed the full-potential linearized-augmented-plane-wave method (WIEN2k package).²⁷ Using the generalized-gradient approximation (GGA)²⁸ we first compare energies of the FM and AFM states of the equilibrium orthorhombic crystal structure and the metastable cubic semi-Heusler structure of CuMnAs and CuMnP. In the former case we use experimental lattice parameters²⁶ $a = 6.5859 \text{ \AA}$, $b = 3.8671 \text{ \AA}$, and $c = 7.3202 \text{ \AA}$ for CuMnAs and $a = 6.3188 \text{ \AA}$, $b = 3.7239 \text{ \AA}$, and $c = 7.0883 \text{ \AA}$ for CuMnP. By minimizing the total energy of the cubic phase we determined the corresponding theoretical lattice constant $a = 5.83 \text{ \AA}$ for CuMnAs and $a = 5.66 \text{ \AA}$ for CuMnP. The calculated

difference between the FM and AFM total energy in the cubic crystal phase is $E_{FM} - E_{AFM} = 52 \text{ meV/Mn-atom}$ for CuMnAs and $E_{FM} - E_{AFM} = 59 \text{ meV/Mn-atom}$ for CuMnP. Here we considered the same AFM alignment of Mn moments in CuMnAs and CuMnP as reported in the neutron diffraction study of CuMnSb.²² A comparison with theoretical results for CuMnSb, where $E_{FM} - E_{AFM} = 50 \text{ meV/Mn-atom}$,¹⁹ suggests that T_N increases when replacing Sb with As or P due to a tighter lattice arrangement. However, the expected increase of T_N is only in the range of $\sim 20\%$ for the cubic phase.

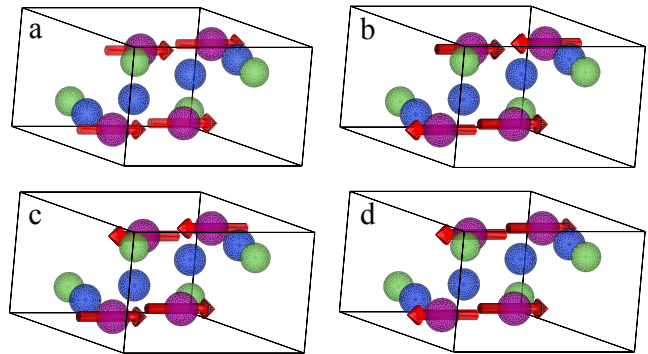


FIG. 1: Color on-line. Atomic and magnetic arrangements of the orthorhombic CuMnAs and CuMnP. Purple (large) spheres with arrows represent Mn, blue (medium) spheres Cu, and green (small) spheres As. (a) FM in-plane arrangement and FM coupling between the planes, (b) AFM in-plane arrangement and FM coupling between the planes, (c) FM in-plane arrangement and AFM coupling between the planes, (d) AFM in-plane arrangement and AFM coupling between the planes.

For the orthorhombic structure we considered the FM and three different AFM moment configurations, as shown in Fig. 1. Mn atoms in these orthorhombic crystals are arranged in layers parallel to the $a - c$ plane and the different AFM arrangements can then be characterized by AFM in-plane arrangement and FM coupling between the planes ($\text{AFM}_{\text{IP-FM}_{\text{OP}}}$, $\text{Pn}'\text{m}'\text{a}$, Fig 1(b)), FM in-plane arrangement and AFM coupling between the planes ($\text{FM}_{\text{IP-AFM}_{\text{OP}}}$, $\text{Pn}'\text{m}'\text{a}'$, Fig 1(c)), or AFM in-plane arrangement and AFM coupling between the planes ($\text{AFM}_{\text{IP-AFM}_{\text{OP}}}$, $\text{Pnm}'\text{a}$, Fig 1(d)). In CuMnAs, the GGA total energies of the $\text{FM}_{\text{IP-AFM}_{\text{OP}}}$ and $\text{AFM}_{\text{IP-AFM}_{\text{OP}}}$ states are very similar (the difference is 1 meV/Mn-atom) while the energy of the $\text{AFM}_{\text{IP-FM}_{\text{OP}}}$ state is significantly higher (by 80 meV/Mn-atom). In CuMnP, the $\text{AFM}_{\text{IP-FM}_{\text{OP}}}$ state has again the highest energy and the difference between the GGA energy of the states $\text{FM}_{\text{IP-AFM}_{\text{OP}}}$ and $\text{AFM}_{\text{IP-AFM}_{\text{OP}}}$ is 30 meV/Mn-atom with the latter AFM state having the lowest energy. When comparing total energies of the FM and AFM states we took the $\text{AFM}_{\text{IP-AFM}_{\text{OP}}}$ state, i.e. compared energies of the spin configurations in Fig. 1(a) and 1(d), and obtained $E_{FM} - E_{AFM} = 241 \text{ meV/Mn-atom}$ for CuMnAs and $E_{FM} - E_{AFM} = 250 \text{ meV/Mn-atom}$ for CuMnP.

atom for CuMnP. These values are significantly larger than in the cubic crystals and the theory, therefore, predicts that the orthorhombic CuMnAs and CuMnP have significantly higher Néel temperature than the semi-Heusler CuMnSb.

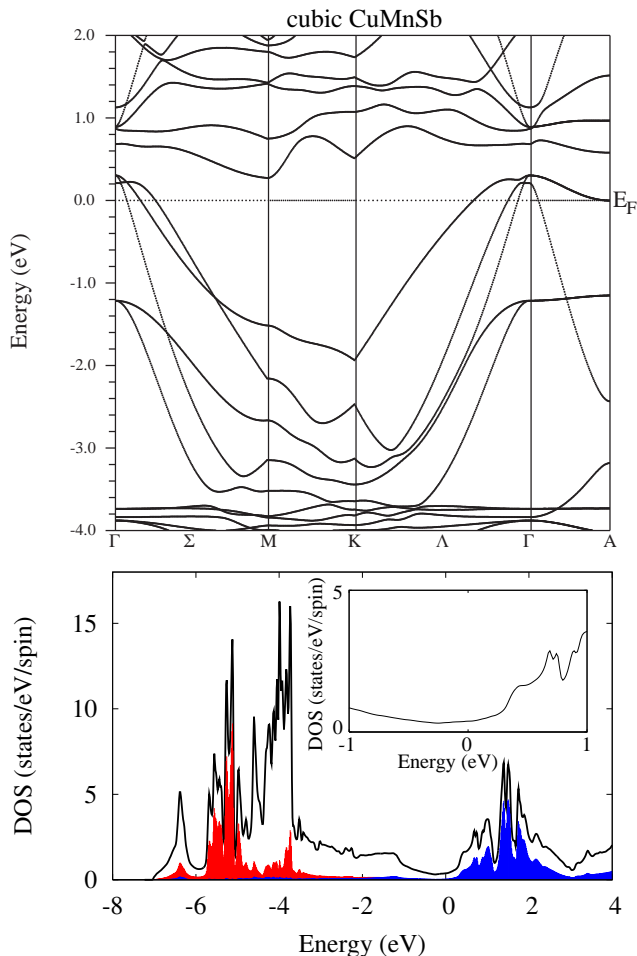


FIG. 2: Color on-line. GGA+U band structure plotted along lines in a hexagonal Brillouin zone (upper panel) and density of states (DOS) of cubic CuMnSb. The red (filled lower energy) data correspond to the DOS projected onto spin-up (spin-down) states of the 1st (2nd) Mn sublattice; the blue (filled higher energy) data correspond to the DOS projected onto spin-down (spin-up) states of the 1st (2nd) Mn sublattice.

The stability of the orthorhombic crystal phase of CuMnAs and CuMnP and the possibility for these compounds to form thin epitaxial films with the metastable cubic phase can be estimated from the difference in total energies of the two crystal structures. For CuMnAs we obtained $E_{cubic} - E_{ortho} = 0.56$ eV/Mn-atom and for CuMnP the difference is $E_{cubic} - E_{ortho} = 1.18$ eV/Mn-atom. For comparison, the total energy of the cubic phase of, e.g., GaN is larger than the energy of the equilibrium hexagonal phase by 0.02 eV/atom and in this case both crystal structures can be realized in thin films. For

MnAs on the other hand, the difference between the cubic and hexagonal phases is 1 eV/Mn-atom and the cubic phase has been stabilized only in the form of nanocrystal inclusions in a cubic matrix. From these comparisons we conclude that the orthorhombic phases of CuMnAs and CuMnP are very stable and the occurrence of the metastable cubic phases in bulk or thin film materials is unlikely.

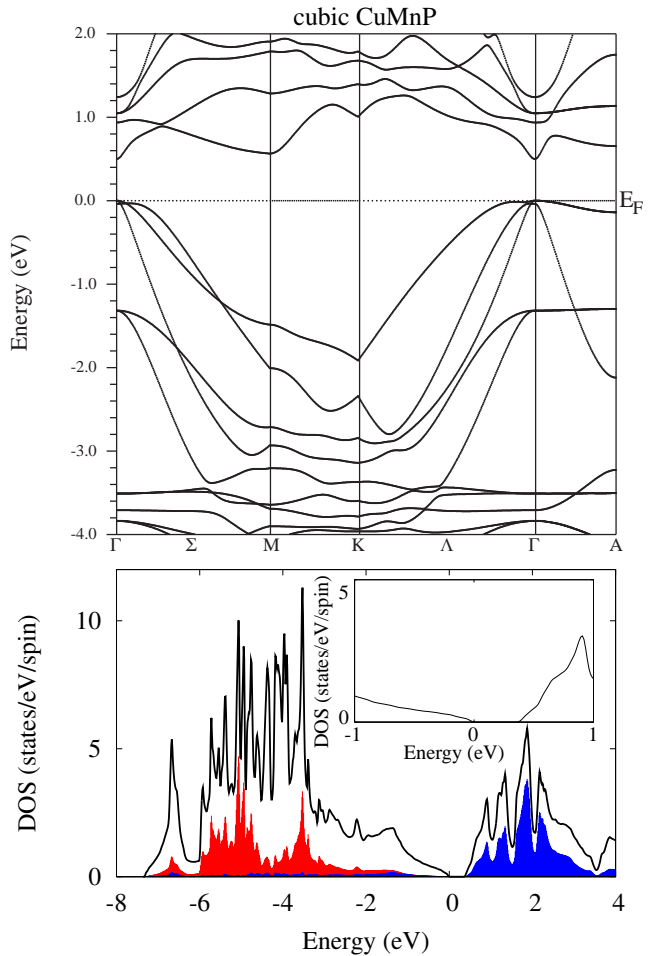


FIG. 3: Same as Fig. 2 for cubic CuMnP.

Examples of the calculated band dispersions are shown in Figs. 2-6. In Figs. 2 and 3 we compare band structures of the cubic CuMnSb and CuMnP calculated in the GGA+U approximations with typical values of the correlation parameters^{29,30} for Mn *d*-orbitals, $U = 3.5$ eV and $J = 0.6$ eV. As already pointed out in Ref. 19, CuMnSb is a semimetal with a negative indirect band-gap. Fig. 3 shows that CuMnP, on the other hand, is already a semiconductor with a fully developed positive band-gap throughout the entire Brillouin zone. The semiconducting band structure of CuMnP is obtained also in the GGA+U calculation of the orthorhombic phase as shown in Fig. 4.

CuMnAs has a small but non-zero density of states at the Fermi energy in the GGA+U spectra as shown in

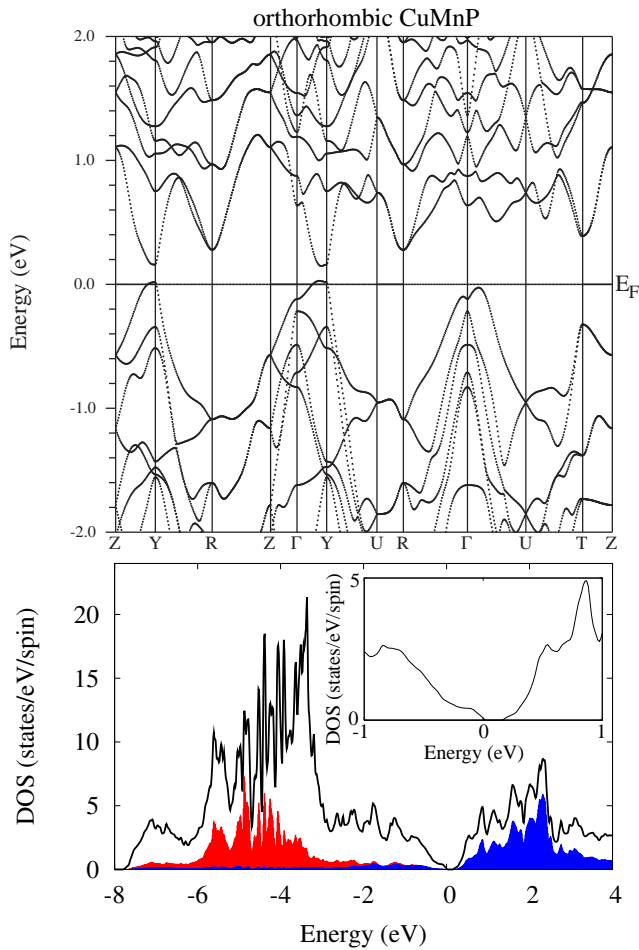


FIG. 4: Color on-line. GGA+U band structure (upper panel) and density of states (DOS) of orthorhombic CuMnP. The red (filled lower energy) data correspond to the DOS projected onto spin-up (spin-down) states of the 1st (2nd) Mn sublattice; the blue (filled higher energy) data correspond to the DOS projected onto spin-down (spin-up) states of the 1st (2nd) Mn sublattice.

Fig. 5. Since density functional theory tends to underestimate band gaps in semiconductors we conclude that the electronic structure of CuMnAs is in the transition region between a semimetal and a semiconductor. For completeness we compare in Fig. 6 band structures of orthorhombic CuMnAs and CuMnP calculated in the local density approximation (LDA),³¹ LDA+U, GGA, and GGA+U. In the plots we focus on the part of the spectra in which the gap opens in CuMnP. The spectra are consistent with common trends in III-V semiconductors of larger band gaps for lighter group-V elements and with the expected enhancement of the calculated semiconductor gap due to both the GGA correction to the local density theory and the correlation effects on Mn *d*-orbitals. Since the effects of these corrections are relatively strong, it might be desirable to employ in future studies computational methods which go beyond the GGA+U approximation in order to get a more quantitative understanding

of the electronic structure of CuMn-V compounds.

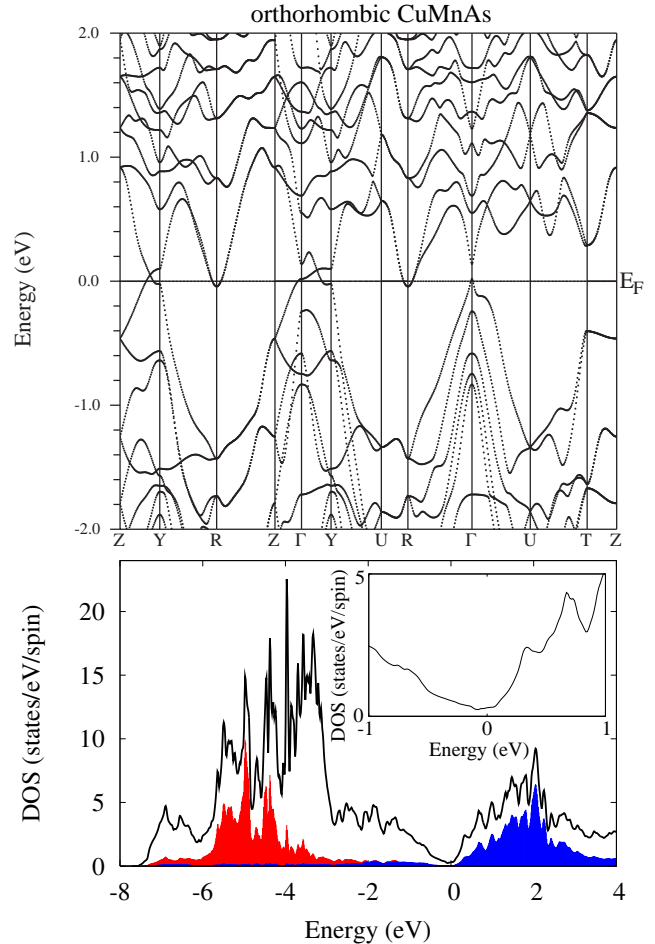


FIG. 5: Same as Fig. 4 for orthorhombic CuMnAs.

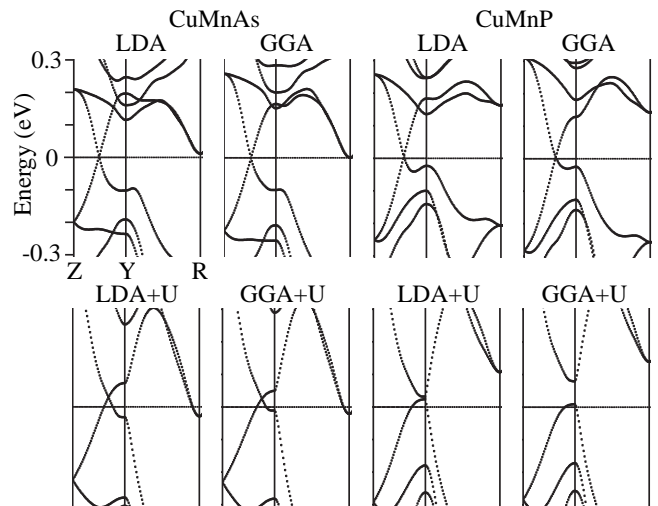


FIG. 6: Band structures of orthorhombic CuMnAs and CuMnP calculated using the depicted density-functional theory models.

III. EXPERIMENT

In this section we discuss experimental properties of CuMnAs. Samples were prepared by direct synthesis from elements mixed in the stoichiometric 1:1:1 ratio using Cu (purity 99.999 %), Mn (purity 99.98 %), and As (purity 99.999 %). They were placed into Al₂O₃ crucible and double sealed inside quartz ampoules. Samples were heated up to 1000°C at a rate of 1°C/min and annealed for 1 day. The reaction produced silver-gray solid rocks. Powder samples and polished-layer samples were prepared from the material for X-ray diffraction measurements, chemical analysis, magnetization measurements by the superconducting quantum interference device (SQUID), van der Pauw transport measurements, and neutron diffraction measurements. For comparison we also prepared CuMnSb samples using the same procedures.

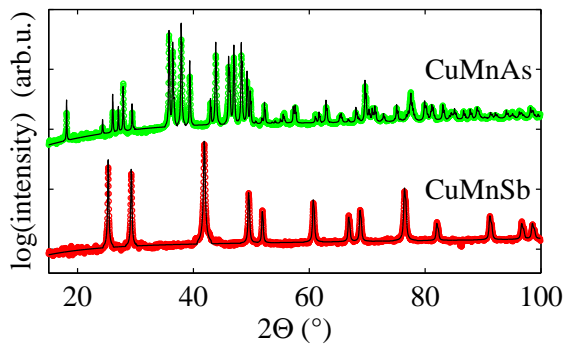


FIG. 7: X-ray diffraction data for CuMnAs and CuMnSb at room temperature. Green points are measured data of CuMnAs, red points are measured data of CuMnSb, and black thin lines are fits considering the orthorhombic crystal structure of CuMnAs and cubic crystal structure of CuMnSb.

In Fig. 7 we show room-temperature X-ray measurements of our CuMnAs and CuMnSb materials. Diffraction patterns were obtained using a Bruker D8 Advance diffractometer in the Bragg-Brentano geometry and copper K_α radiation. Data analysis was carried out using the FullProf package.³² The measurements show that CuMnAs has the orthorhombic Pnma crystal structure consistent with X-ray data in Ref. 26 and CuMnSb has the cubic semi-Heusler structure as reported previously.²³ Note that X-ray measurements of CuMnAs performed in the 300 K - 600 K range did not reveal any structural phase transition. Elemental analysis by energy-dispersive X-ray spectroscopy (EDX) confirmed the stoichiometric 1:1:1 ratio of Cu, Mn, and As(Sb) in the studied materials within the experimental error of ~1%.

In Fig. 8 we show measurements of the temperature dependent susceptibility and field dependent magnetization in CuMnSb. The data indicate $T_N \approx 50$ K, in agreement with previous reports on this material.²³ Analogous measurements in CuMnAs are presented in Fig. 9. We observe that the magnetic susceptibility of CuMnAs in-

creases with increasing temperature up to much higher temperatures than in CuMnSb, in agreement with measurements presented in Ref. 26. The dependence reverses above ~450 K, indicating that T_N is above room temperature. As in the AFM CuMnSb we observe zero remanence below T_N in CuMnAs (see inset in Fig. 9).

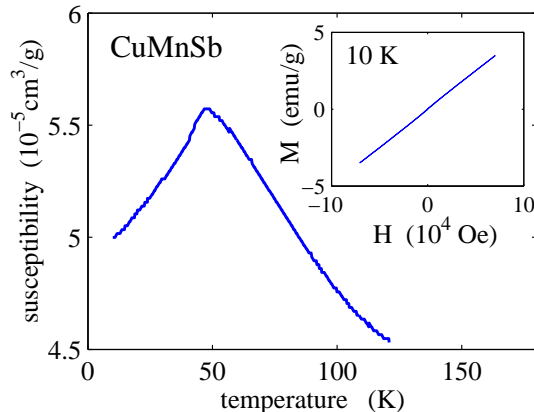


FIG. 8: Magnetic susceptibility at 5 kOe of CuMnSb. Inset shows magnetization measured at 10 K.

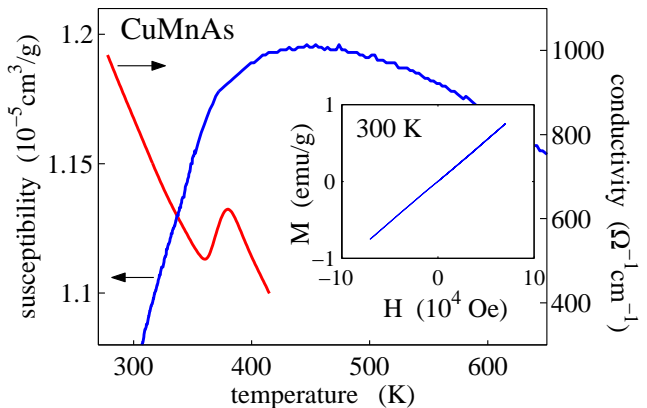


FIG. 9: Magnetic susceptibility at 5 kOe and conductivity of CuMnAs. Inset shows magnetization measured at 300 K.

The transition to a magnetically ordered state in CuMnAs is observed also in transport data shown in Fig. 9. Above 400 K the material has a metallic conductance which increases with decreasing temperature. Near 400 K the conductance drops abruptly before it resumes the metallic character below 350 K. Such a conductance drop is commonly observed in magnetic materials and associated with critical scattering near the transition temperature. We also point out that the conductivity at 300 K of CuMnAs is $800 \Omega^{-1} \text{cm}^{-1}$ which is almost an order of magnitude lower than the room-temperature conductivity of the semimetal CuMnSb. This is consistent with the theoretically predicted trend towards semiconducting character of CuMn-V compounds with lighter group-V elements.

We conclude the experimental section by presenting

initial results of room-temperature neutron diffraction measurements. The data shown in Fig. 10 were taken on the instrument MEREDITH in the Nuclear Physics Institute in Rez, Czech Republic. The neutron beam was monochromatized by a copper mosaic monochromator to a wavelength of 1.46 Å. The data show evidence of magnetic order at room temperature. The best fit using FullProf package³² to the data was obtained for the AFM_{IP}-AFM_{OP} Mn moment configuration (Fig 1(d)).

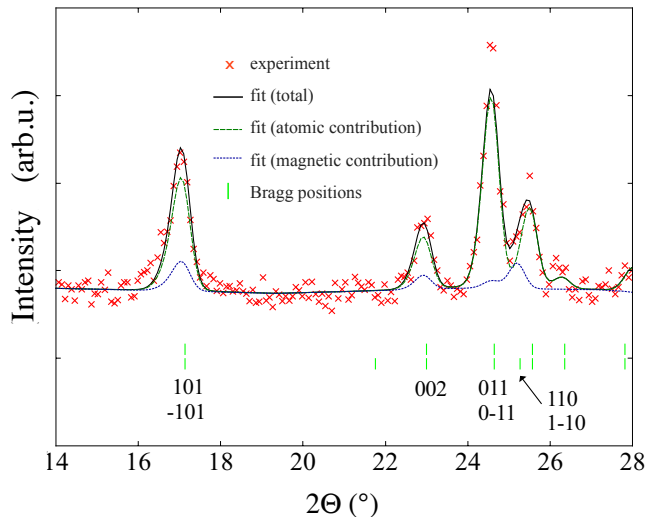


FIG. 10: Low angle part of measured and fitted neutron diffraction data of CuMnAs at room temperature. Atomic and magnetic contributions are plotted separately. Bragg positions of atomic (top) and magnetic (bottom) structures are also highlighted. Crystallographic indices denote the magnetic phase related reflections. The peak in the magnetic contribution highlighted by arrow is characteristic of the AFM_{IP}-AFM_{OP} Mn moment configuration.

IV. SUMMARY

In summary, we have performed a combined theoretical and experimental study of electronic and magnetic properties of CuMn-V compounds which complements previous work on alkali-metal based I(a)-Mn-V AFM semiconductors. The transition from a low Néel temperature AFM CuMnSb to room-temperature AFMs CuMnAs and CuMnP is ascribed to the orthorhombic crystal structure of the latter two compounds. The transition from a semimetal CuMnSb to a semiconductor CuMnP is reminiscent of the trend of increasing band gap in III-V semiconductor compounds with lighter group-V elements. Since CuMn-V compounds are stable and readily compatible with common epitaxial growth techniques of high-quality semiconductor structures, they might represent favorable systems for exploring the concept of AFM-based spintronics.

Acknowledgment

We thank C. Frontera and V. Holý for useful discussions and M. Maryško for experimental assistance and we acknowledge support from EU Grant FP7-215368 SemiSpinNet, and ERC Advanced Grant 268066, from Czech Republic Grants P204/11/P339, AV0Z10100520, AV0Z10100521, IAA100100912, LC510, and Preamium Academiae.

- ¹ A. B. Shick, S. Khmelevskiy, O. N. Mryasov, J. Wunderlich, and T. Jungwirth, *Phys. Rev. B* **81**, 212409 (2010).
- ² B. G. Park, J. Wunderlich, X. Marti, V. Holy, Y. Kurosaki, M. Yamada, H. Yamamoto, A. Nishide, J. Hayakawa, H. Takahashi, et al. (2010).
- ³ E. L. Nagaev, *Sov. Phys. Usp.* **18**, 863 (1975).
- ⁴ K. Suzuki, H. Morita, T. Kaneko, H. Yoshida, and H. Fujimori, *J. Alloys Compd.* **201**, 11 (1993).
- ⁵ X. Chen, A. Hochstrat, P. Borisov, and W. Kleemann, *Appl. Phys. Lett.* **94**, 032506 (2009).
- ⁶ B. Westerstrandh, L. Lundgren, U. Gafvert, and B. Carlsson, *Phys. Scr.* **15**, 276 (1977).
- ⁷ K. Selte, A. Kjekshus, and A. Andresen, *Acta Chem. Scand.* **26**, 3101 (1972).
- ⁸ P. J. Picone, a, and P. E. Clark, *J. Magn. Magn. Mater.* **25**, 140 (1981).
- ⁹ E. Kaldis, G. von Schulthess, and P. Wachter, *Solid State Commun.* **17**, 1401 (1975).
- ¹⁰ D. X. Li, Y. Haga, H. Shida, T. Suzuki, T. Koide, and G. Kido, *Phys. Rev. B* **53**, 8473 (1996).
- ¹¹ F. P. Missell, R. P. Guertin, and S. Foner, *Solid State Commun.* **23**, 369 (1977).
- ¹² M. Mekata, N. Yaguchi, T. Takagi, T. Sugino, S. Mitsuda, H. Yoshizawa, N. Hosoito, and T. Shinjo, *J. Phys. Soc. Jpn.* **62**, 4474 (1993).
- ¹³ S. Esmailzadeh, U. Halenius, and M. Valldor, *Chem. Mater.* **18**, 2713 (2006).
- ¹⁴ J. Lamazares, F. Gonzalez-Jimenez, E. Jaimes, L. D'Onofrio, R. Iraldi, G. Sanchez-Porras, M. Quintero, J. Gonzalez, J. C. Woolley, and G. Lamarche, *J. Magn. Magn. Mater.* **104-107**, 997 (1992).
- ¹⁵ A. Rivas, F. Gonzalez-Jimenez, L. D'Onofrio, E. Jaimes, M. Quintero, and J. Gonzalez, *Hyperfine Interactions* **113**, 493 (1998).
- ¹⁶ T. Jungwirth, V. Novák, X. Marti, M. Cukr, F. Máca, A. B. Shick, J. Mašek, P. Horodyská, P. Němec, V. Holý, et al., *Phys. Rev. B* **83**, 035321 (2011).
- ¹⁷ W. Bronger, P. Müller, R. Höppner, and H. U. Schuster, *Z. Anorg. Allg. Chem.* **539**, 175 (1986).
- ¹⁸ F. Schucht, A. Dascalidou, R. Muller, W. Jung, H. U.

- Schuster, W. Bronger, and P. Muller, *Z. Anorg. Allg. Chem.* **625**, 31 (1999).
- ¹⁹ T. Jeong, R. Weht, and W. E. Pickett, *Phys. Rev. B* **71**, 184103 (2005).
- ²⁰ I. Galanakis, E. Sasioglu, and K. Özdoğan, *Phys. Rev. B* **77**, 214417 (2008).
- ²¹ J. Boeuf, C. Pfeleiderer, and A. Faisst, *Phys. Rev. B* **74**, 024428 (2006).
- ²² R. H. Forster, G. B. Johnston, and D. A. Wheeler, *J. Phys. Chem. Solids* **29**, 855 (1968).
- ²³ K. Endo, *J. Phys. Soc. Jpn.* **29**, 643 (1970).
- ²⁴ S. S. Abdulnoor, F. M. J. Ali, and J. Leciejwicz, *J. Magn. Magn. Mater.* **15-18**, 475 (1980).
- ²⁵ N. P. Duong, L. T. Hunga, T. D. Hiena, N. P. Thuy, N. T. Trung, and E. Brück, *J. Magn. Magn. Mater.* **311**, 605 (2007).
- ²⁶ J. Müdelein and H. U. Schuster, *Z. Naturforsch. B* **47**, 925 (1992).
- ²⁷ P. Blaha, K. Schwarz, G. K. H. Madsen, D. Kvasnicka, and J. Luitz, *An Augmented Plane Wave + Local Orbitals Program for Calculating Crystal Properties*, ISBN 3-9501031-1-2 (Karlheinz Schwarz, Techn. Universität Wien, Austria, 2001).
- ²⁸ J. P. Perdew, K. Burke, and M. Ernzerhof, *Phys. Rev. Lett.* **77**, 3865 (1996).
- ²⁹ V. I. Anisimov, I. V. Solovyev, M. A. Korotin, M. T. Czyzyk, and G. A. Sawatzky, *Phys. Rev. B* **48**, 16929 (1993).
- ³⁰ A. I. Liechtenstein, V. I. Anisimov, and J. Zaanen, *Phys. Rev. B* **52**, R5467 (1995).
- ³¹ J. P. Perdew and Y. Wang, *Phys. Rev. B* **45**, 13244 (1992).
- ³² J. Rodríguez-Carvajal, *Physica B* **192**, 55 (1993).